Experimental investigation of meandering jets in shallow reservoirs

Y. Peltier [1], S. Erpicum, P. Archambeau, M. Pirotton & B. Dewals

University of Liege (ULg), ArGEnCo Department, Research Group HECE. Chemin des Chevreuils 1, Bat B52/3 +1, 4000, Liège, Belgium.

Abstract

Meandering flows in rectangular shallow reservoirs were experimentally investigated. The characteristic frequency, the longitudinal wave length and the mean lateral extension of the meandering jet were extracted from the first paired modes, obtained by a Proper Orthogonal Decomposition (POD) of the surface velocity field measured by Large Scale PIV (LSPIV). The depth-normalised characteristic lengths and the Strouhal number were then compared to the main dimensionless numbers characterizing the experiments: Froude number, friction number and reservoir shape factor. The normalised wave length and mean lateral extension of the meandering jet are neither correlated with the Froude number nor with the reservoir shape factor; but a clear relationship is found with the friction number. Similarly, the Strouhal number is found proportional to a negative power of the friction number. In contrast, the Froude number and the reservoir shape factor enable to predict the occurrence of a meandering flow pattern: meandering jets occur for Froude number greater than 0.21 and for a shape factor smaller than 6.2.

Keywords

Shallow reservoir, meandering jet, Proper Orthogonal Decomposition, Large-Scale PIV

1. INTRODUCTION

Shallow reservoirs are common in hydraulic engineering. They are used for water storage

[1] Corresponding author: yann.peltier90@gmail.com, Phone: +32 4 366 92 67, Fax: +32 4 366 95 58

or sediment trapping. From an operational point of view, predicting accurately the amount and the location of the sediment deposits is of high importance. The quality of this prediction is strongly dependent on the detailed knowledge of the flow field developing within the reservoir [1,2].

Recent studies emphasized the complexity of flows in rectangular shallow reservoirs [3-5]. The jet developing at the entrance of the reservoir can either be straight from the inlet to the outlet, or can impact one or several times the lateral walls. Using the shape factor, $\mathsf{SF} = L/\Delta B^{0.6} b^{0.4}$ (L the reservoir length, b the width of the inlet channel and ΔB the width of the sudden expansion), Dufresne et al. [5] showed that for $\mathsf{SF} < 6.2$ the flow patterns are symmetric, for $\mathsf{SF} > 6.8$ they are asymmetric, and for $6.2 < \mathsf{SF} < 6.8$ both types of flow patterns may be observed.

In his PhD Thesis at EPFL, Kantoush (2008) [6] revealed the existence of symmetric flows with temporal and spatial periodical oscillations of the jet when $\mathsf{SF} = 7.2$, $\mathsf{F} > 0.1$ (F the Froude number) and $H/\Delta B < 0.2$ ($H/\Delta B$ the shallowness parameter and H the mean water depth in the reservoir). He named these flows as “meandering”, but no quantitative characterisation of the jets was made (neither their frequency nor their characteristics lengths) to really confirm the meandering behaviour of these flows. More recently, Camnasio et al. (2012) [7] performed visual observations of meandering jets, but again without quantitative experimental characterisation, and showed that a 2D depth-averaged flow model can simulate the occurrence of meandering jets.

The study of these meandering flows is of high relevance for reservoir management (*e.g.*, for the prediction of reservoir trapping efficiency and of the spatial pattern of sediment deposits …). This “meandering” behaviour is responsible for the generation of large-scale vortices on both sides of the jet, which transfer momentum from the jet towards the rest of the reservoir and induce significant changes in the velocity distribution compared to a configuration without meandering jet [8]. Using the numerical modelling WOLF 2D [3,9], Peltier et al. [8] showed that these changes in the velocity distribution have a strong impact on the sediment transport and deposition. Indeed, the meandering jet induces a larger spreading of the sediments on both sides of the jet, which increases the reservoir trapping efficiency. A two-way coupling may also be observed between the flow and the sediment transport, since bathymetric changes due to sediment deposits may induce changes in the flow pattern [9].

The purpose of this paper is to present a first experimental characterization of these meandering flows in short rectangular shallow reservoirs. The experimental setup is first described and the key parameters of the problem are identified by a dimensional analysis. Next, the influence of these parameters on the characteristics of the meandering flow (frequency, longitudinal wave length and mean lateral extension of the jet) is analysed. Finally the correlations found between the characteristics of the meandering jet and the other parameters are discussed.

2. MATERIAL AND METHODS

2.1. Experimental device

The experiments were carried out at the laboratory of engineering hydraulics of the University of Liege (ULg), Belgium as shown in Fig. 1. The experimental flume consists in a 10.40 m long and 0.98 m wide glass channel, in which blocks can be arranged to build different geometries of rectangular reservoirs. The bottom of the flume is horizontal. The flow enters the channel from a stilling basin through a porous screen in order to prevent fluctuations in water level and to facilitate the establishment of a fully developed velocity profile. The flow is then contracted to the width of the inlet channel, b, through a converging section. The inlet channel is 2.00 m long and has straight parallel walls. At the entrance of the reservoir, the flow suddenly expands to the width of the reservoir, $B=b+2\times\Delta B$. At the exit of the reservoir, the flow suddenly contracts to the outlet channel width, which is the same as in the inlet channel. The outlet channel is 1.50 m long and it ends with a tailgate and a control weir. All the surfaces are made of glass, except the bottom of the flume (PVC) and the converging section (metallic sheets).

The discharge, Q, was measured with an electromagnetic flowmeter (uncertainty of 0.025 L/s) mounted on the pipe connecting the downstream tank to the upstream tank. The discharge was regulated to ensure the temporal stability of the supply. This regulation was ensured through a pressure sensor mounted on the pump and an overflow system, which enabled to keep constant the head at the entrance of the pump (constant water level in the downstream tank).

The water depth was measured using an ultrasonic probe and the surface velocity as well as the vortex dynamics was measured by LSPIV [10,11]. The uncertainty on the water depth was estimated to 1% of the mean value. The uncertainty on the mean velocity was estimated to 5%.

2.2. Dimensional analysis

Meandering jets in rectangular shallow reservoirs can be described based on 14 independent parameters (Tab. 1) and the number of dimensions of such a problem is 3 (Length = H, Time H^3/Q, Mass = ρH^3). As a result, the number of Π-parameters is equal to 14-3 = 11 (see Tab. 1).

The Π-parameters in Tab. 1 are classified into three groups: geometry, hydraulics and fluid. For the Π-parameters related to the hydraulics and the fluid, the choice of H for expressing the length-scale, instead of the width b or ΔB, is driven by the observations of Dracos et al. [12], who showed that the behaviour of a plane turbulent jet in a bounded fluid layer is better explained when the dimensional analysis is based on the depth of the fluid layer rather than the width of the orifice. Nevertheless, for the geometry, we combined the Π-parameters 1-3 in order to come up with standard non-dimensional parameters in the literature for characterizing the reservoir geometry ($\Delta B/L$, $b/\Delta B$).

Focusing on the characteristics of the meandering jet, the parameters Π_6, Π_7 and Π_8 can be expressed as a function of all other Π-parameters:

$$\left(\mathsf{St}, \frac{\Lambda_x}{H}, \frac{\Lambda_y}{H}\right) = \mathbb{F}\left(\frac{H}{\Delta B}, \frac{\Delta B}{L}, \frac{b}{\Delta B}, \frac{\varepsilon}{H}, S_o, \mathsf{R}, \mathsf{F}, \mathsf{W}\right) \tag{1}$$

The friction coefficient, λ, as deduced from a friction formula such as Colebrook-White, is a function of the roughness, ε, and of the Reynolds number R. Consequently, we assumed that the influence of ε and R is lumped into the friction coefficient λ.

Using the friction coefficient and the shallowness parameter $H/\Delta B$, a friction number can be obtained for flows in shallow reservoirs [5], similarly to the expression introduced by Chu et al. [13]:

$$\mathsf{S} = \frac{\lambda \Delta B}{8H} \tag{2}$$

As a result, Eq. 1 reduces to:

$$\left(\mathsf{St}, \frac{\Lambda_x}{H}, \frac{\Lambda_y}{H}\right) = \mathbb{F}\left(\frac{\Delta B}{L}, \frac{b}{\Delta B}, S_o, \mathsf{S}, \mathsf{F}, \mathsf{W}\right) \tag{3}$$

Since most real-world reservoirs configurations have no significant slope, the present experimental study focuses on reservoirs with a horizontal bottom and therefore the influence of S_o can be neglected. In addition, using the shape factor, $\mathsf{SF} = \Pi_3^{-0.4} / \Pi_1 = L/\Delta B^{0.6} b^{0.4}$ as defined by Dufresne et al. [5], Eq. 3 can be simplified as follows:

$$\left(\mathsf{St}, \frac{\Lambda_x}{H}, \frac{\Lambda_y}{H}\right) = \mathbb{F}\left(\mathsf{SF}, \mathsf{S}, \mathsf{F}, \mathsf{W}\right) \tag{4}$$

In the present experiments, the free surface deformations remain low (1 or 2 mm). As a consequence, the Weber number, W, is expected to have little influence on the development of the flow. The only way of verification would be to compare results from models of different scales, which was not possible here. As a consequence, we decided to neglect Weber number in our analysis and Eq. 1 finally reduces to:

$$\left(\mathsf{St},\frac{\Lambda_x}{H},\frac{\Lambda_y}{H}\right)=\mathbb{F}\left(\mathsf{SF},\mathsf{S},\mathsf{F}\right) \tag{5}$$

2.3. Experimental data set

Different hydraulic and geometric configurations were considered to enable the observation of a wide range of meandering flows (Tab. 2). Two inlet channel widths and five lengths of reservoir were tested. Three different crest heights were used in order to obtain various water depths for a given discharge. For each combination of geometry and crest height, at least five different discharges were used and all experiments were repeated 2 to 3 times. The resulting Froude, friction and Reynolds numbers of the whole set of experiments are summarized in Tab. 2. The Froude numbers lay between 0.08 and 0.53. The Friction number is between 0.01 (non-frictional regime, see Chu et al. [14]) and 0.24 (frictional regime), which indicates that various types of coherent structures are expected in the experiments and therefore various behaviours of the jet. The Reynolds number is between 7,200 and 65,700, which emphasizes that the jet can be considered as turbulent. Given these Reynolds numbers, the flows are hydro-dynamically smooth. This justifies the necessity of considering both the Reynolds number and the roughness for estimating the friction number as noticed in section 2.2. Among all the tested geometric and hydraulic conditions, 50 distinct configurations out of 80 led to a meandering flow.

For thirty nine of these meandering jets (see Tab. 3 in appendix), the instantaneous surface velocity field was measured by LSPIV and a Proper Orthogonal Decomposition

(POD) analysis [15] was performed on these fields to extract the frequency, the wave length and the mean lateral extension of the meandering jet. The process to extract these characteristics is schematized in Fig. 2. For each experiment, seeds of 2 mm of mean diameter were first placed on the surface of the flow and a field of 1 m × 1 m, containing the entrance of the reservoir, was video recorded at a rate of 25 Hz during at least 7’30’’ using a commercial video-camera (Canon© HD-HG20). After extraction from the video, correction and orthorectification of the images to be processed [16], one pixel was equal to a square of 1 mm side. Using a homemade LSPIV code based on the work of Hauet [16], the surface velocity fields were worked out on a square mesh of 1 cm × 1cm.

The POD analysis was then performed on the surface velocity fields in order to identify the most energetic structures characterizing the meandering flow.

- The POD analysis emphasized the existence of pairs of modes with similar patterns: the temporal modes are similar, but phase-shifted in time, while the spatial modes are shifted in space (Fig. 2). This indicates that both modes in a pair are directly related to the same coherent structure [17].
- By definition of the POD [15], the first paired modes corresponding to the meandering jet are the most energetic ones (modes 1 & 2) or are among the most energetic modes (modes 2 & 3 or modes 3 & 4), the first modes representing in the latter case a very energetic slow motion of the jet.

A 1D Fourier analysis was finally performed on the identified modes for extracting the characteristic frequency, f_{max}, of the most energetic oscillations and the characteristic lengths of the jet in the longitudinal direction (Λ_x, wave length of the meander) and in the lateral direction (Λ_y, mean lateral extension of the structures in the jet). For extracting the characteristic frequency, the Fourier analysis was performed on the temporal modes. The characteristic lengths were identified using a Fourier analysis made on the vorticity field deduced from the spatial modes (Fig. 2):

- Λ_x is the inverse of the wave number corresponding to the maximum of the spectrum of the longitudinal distribution of the vorticity field within an interval of five centimetres on both sides of the reservoir centreline,
- Λ_y is the mean of the inverses of the wave numbers corresponding to the maximums of the spectrum of the distribution of vorticity in each cross-section.

3. RESULTS

3.1. Normalised characteristic lengths

The normalised characteristic lengths Λ_x/H and Λ_y/H are plotted against S, F and SF in Fig. 3. There is no simple relationship between the normalised characteristic lengths and the Froude number nor the shape factor (Fig. 3a). In contrast, the dependence of the normalised characteristic lengths on the friction number shows a distinctive linear distribution for Λ_x/H on the whole range of S and a power-law distribution for Λ_y/H (Fig. 3b). Based on a total least square fitting (variables on both abscesses are considered as random) [18]; these distributions can be approximated as follows:

$$\frac{\Lambda_x}{H} = 145 \times \mathsf{S} + 2.4 \ \ (R^2 = 0.85) \tag{6}$$

$$\frac{\Lambda_y}{H} = 20 \times \mathsf{S}^{0.45} \ \ (R^2 = 0.62) \tag{7}$$

R^2 being the linear standard coefficient of determination calculated with S and Λ_x/H for Eq. 6 and calculated with $\log(\mathsf{S})$ and $\log(\Lambda_y/H)$ for Eq. 7.

Multiplying Eq. 6 by H and using Eq. 2 indicate that the longitudinal characteristic length (*i.e.* the meandering wave-length) is mostly proportional to the product $\lambda \times \Delta B$ for high values of S and to the water depth H for relatively low values of S.

Eq. 7 highlights the existence of an attenuation of the growth rate of Λ_y/H with increasing S. Moreover, multiplying Eq. 7 by H and using Eq. 2 reveal that the mean lateral extension of the jet is almost proportional to the square root of $\lambda \times \Delta B \times H$. The dependency to the water depth suggests that a vertical confinement operates on the jet. This is consistent with the observations of Chu et al. [14], which reveal that, for small S values (*i.e.* H is high relative to the dimension of the experiment), the lateral spreading of the jet is mainly driven by a large scale turbulence (non-frictional regime) with a characteristic length scale proportional to $\lambda \times \Delta B$, whereas for high values of S (*i.e.* H is small), the lateral spreading of the jet is driven by the bottom generated turbulence, with a characteristic length-scale proportional to H.

When considering the ratio of Λ_x and Λ_y as a function of S (Fig. 4), no correlation can be found when $S < 0.07$, which corresponds to the upper limit of the non-frictional regime [14]. In contrast for $S > 0.07$, a linear relationship can be found and follows Eq. 8.

$$\frac{\Lambda_x}{\Lambda_y} = 6.83 \times S + 1.61 \;\; (R^2 = 0.65) \tag{8}$$

R^2 being the linear standard coefficient of determination calculated with S and Λ_x/Λ_y.

3.2. Strouhal number

The Strouhal number, which is representative of the characteristic frequency f_{max}, is plotted against F and SF in Fig. 5a. No clear correlation is found between St, F and SF. Data are too scattered to identify a clear tendency. In contrast, a clear dependency is found between St and S (Fig. 5b). Indeed, the Strouhal number can be expressed as a function of the friction number as follows:

$$St = 0.004 \times S^{-0.776} \;\; (R^2 = 0.66) \tag{9}$$

R^2 being the linear standard coefficient of determination calculated with log(S) and log(St).

Eq. 9 indicates that the vortex shedding within the jet is attenuated by the vertical confinement resulting from lower water depths. The meandering of the flow is also weakened by an increase in the friction effects.

4. DISCUSSION

In the previous section, we showed that the normalised characteristics of the meandering flows are mainly related to the friction number and they are neither directly affected by the shape factor nor by the Froude number (Tab. 2).

To further explore the role of F and SF, the present data (Tab. 2) and the data of [4,5,6] were plotted altogether in Fig. 6. Four types of flow can be distinguished:

1. Meandering flows
2. Instable flows: the flow was alternatively meandering or symmetric/asymmetric during the same experiment
3. Symmetric flows: the jet was straight all along the experiment
4. Asymmetric flows: the jet impacts one or several times the lateral wall of the reservoir

The distribution of the data points in Fig. 6 reveals that the Froude number F and the slope factor SF enable to clearly define the respective domains of occurrence of each type of flow. The meandering flows are defined for $\mathsf{F} > 0.21$ and $\mathsf{SF} < 6.2$. The symmetric flows are defined for $\mathsf{F} < 0.21$ and $\mathsf{SF} < 6.2$ (horizontal line in Fig. 6), while the asymmetric flows exist for $\mathsf{SF} > 6.2$-8.1 with no restriction on the Froude number value. The instable regime is observed for $6.2 < \mathsf{SF} < 8.1$, especially $\mathsf{F} > 0.21$.

5. CONCLUSION

The present paper investigates meandering flows in shallow rectangular reservoirs. Fifty meandering jets were identified amongst a data set of 80 jets in shallow rectangular reservoirs.

For thirty nine of these meandering jets, the instantaneous surface velocity field was measured and a POD analysis was performed on these fields to extract their main characteristics (frequency, wave length and mean lateral extension of the meandering jet).

The characteristic lengths of the meandering jet were normalised by the mean water depth in the reservoir and the frequency was written in the form of a Strouhal number. They were then compared to the shape factor of the reservoir, to the Froude number and to the friction number evaluated at the reservoir inlet.

No correlation is found between the shape factor, the Froude number and the characteristic parameters of the meandering jet, but the comparison of the present data-set with past experiments emphasizes that the shape factor defines the upper-limit of existence of the symmetrical flows ($\mathsf{SF} \leq 6.2$) and the Froude number enables to identify the limit, above which the jet meanders ($\mathsf{F} > 0.2$).

Nevertheless, correlations are found between the friction number and the characteristic parameters of the meandering jet. The depth-normalised wave length of the meander varies linearly with the friction number, which indicates that the wave length of the meander grows with the reservoir width and/or friction coefficient. The depth-normalised mean lateral extension of the jet is almost proportional to the square root of the friction number. It results that the mean lateral extension is affected by the water depth; a vertical confinement of the jet occurs and affects the lateral spreading of the jet at high values of S (*i.e.* at low water depth). Finally, the Strouhal number is proportional to a negative power of the friction number, which emphasizes a damping of the meandering for increasing friction or decreasing water depth.

Future research should confirm whether the present findings remain valid in the case of a rough bottom, as encountered in more realistic configurations.

6. ACKNOWLEGMENTS

The research was funded by the University of Liège (grant SFRD-12/27). The authors are grateful for the assistance provided by the research technicians during the experiments and the fruitful discussions about the POD analysis with Prof. Vincent Denoël.

7. REFERENCES

1. Dufresne M, Dewals BJ, Erpicum S, Archambeau P, Pirotton M (2010) Experimental investigation of flow pattern and sediment deposition in rectangular shallow reservoirs. International Journal of Sediment Research 25 (3):258-270

2. Dufresne M, Dewals B, Erpicum S, Archambeau P, Pirotton M (2012) Flow patterns and sediment deposition in rectangular shallow reservoirs. Water and Environment Journal

3. Dewals BJ, Kantoush SA, Erpicum S, Pirotton M, Schleiss AJ (2008) Experimental and numerical analysis of flow instabilities in rectangular shallow basins. Environmental Fluid Mechanics 8 (1):31-54

4. Camnasio E, Orsi E, Schleiss AJ (2011) Experimental study of velocity fields in rectangular shallow reservoirs. Journal of Hydraulic Research 49 (3):352-358

5. Dufresne M, Dewals BJ, Erpicum S, Archambeau P, Pirotton M (2010) Classification of flow patterns in rectangular shallow reservoirs. Journal of Hydraulic Research 48 (2):197-204

6. Kantoush SA (2008) Experimental study on the influence of the geometry of shallow reservoirs on flow patterns and sedimentation by suspended sediments. Ph. D. thesis, No 4048, EPFL, Lausanne

7. Camnasio E, Pirotton M, Erpicum S, Dewals B Experimental and numerical investigation of a meandering jet in shallow rectangular reservoirs under different hydraulic conditions. In: 3rd International Symposium on Shallow Flows, Iowa City, USA, June 4-6 2012.

8. Peltier Y, Erpicum S, Archambeau P, Pirotton M, Dewals B (2013) Experimental and numerical investigation of meandering jets in shallow reservoir: potential impacts on deposit patterns. Paper presented at the THESIS 2013, Two-pHase modElling for Sediment dynamIcs in Geophysical Flows, Chatou, France, 10-12 June

9. Camnasio E, Erpicum S, Orsi E, Pirotton M, Schleiss AJ, Dewals B (2013) Coupling between flow and sediment deposition in rectangular shallow reservoirs. Journal of Hydraulic Research. doi:10.1080/00221686.2013.805311

10. Hauet A, Kruger A, Krajewski WF, Bradley A, Muste M, Creutin JD, Wilson M (2008) Experimental system for real-time discharge estimation using an image-based method. Journal of Hydrologic Engineering 13 (2):105-110. doi:10.1061/(ASCE)1084-0699(2008)13:2(105)

11. Kantoush SA, Schleiss AJ (2009) Large-scale piv surface flow measurements in shallow basins with different geometries. Journal of Visualization 12 (4):361-373

12. Dracos T, Giger M, Jirka GH (1992) Plane turbulent jets in a bounded fluid layer. Journal of Fluid Mechanics 241:587-614

13. Chu VH, Khayat RE, Wu JH (1983) Stability of turbulent shear flows in shallow channel. In: 20th IAHR Congr., Sep. 5-9, Moscow, USSR, 1983. Delft, The Netherlands, IAHR, pp 128-133

14. Chu VH, Liu F, Altai W (2004) Friction and confinement effects on a shallow recirculating flow. Journal of Environmental Engineering and Science 3 (5):463-475. doi:10.1139/S04-034

15. Holmes P, Lumley JL, Berkooz G, Rowley CW (2012) Turbulence, Coherent Structures, Dynamical Systems and Symmetry. Second Edition. Cambridge Monographs on Mechanics, 2nd edn. Cambridge University Press

16. Hauet A (2009) Discharge estimate and velocity measurement in river using Large-Scale Particle Image Velocimetry; Estimation de débit et mesure de vitesse en rivière par Large-Scale Particle image Velocimetry. La Houille Blanche (1):80-85. doi:10.1051/lhb.2009009

17. Rempfer D, Fasel HF (1994) Evolution of three-dimensional coherent structures in a flat-plate boundary layer. Journal of Fluid Mechanics 260:351-375

18. Van Huffel S (2004) Total Least Squares and Errors-in-Variables Modeling: Bridging the Gap between Statistics, Computational Mathematics and Engineering. K.U.Leuven, Dept. of Electrical Engineering (ESAT), Research Group SCD (SISTA)

8. APPENDIX

In Tab. 3, the geometric and hydraulic conditions of the thirty nine meandering flows are summarized

Tab. 1 Dimensional analysis: variables and Π-parameters

Types	Variables		Π-parameters	
Geometry	Length of the reservoir	L	$\Pi_1 = H / L \times \Pi_2^{-1} = \Delta B / L$	
	Width of the lateral expansion	ΔB	$\Pi_2 = H / \Delta B$	Shallowness
	Width of the inlet and outlets channels	b	$\Pi_3 = b / H \times \Pi_2 = b / \Delta B$	Protrusion ratio
	Slope of the reservoir	S_o	$\Pi_4 = S_o$	
Hydraulics	Discharge	Q	Variable used for expressing the dimensions of the problem	
	Velocity at the inlet	V	Dependent Variable: $V = Q / \left(bH\right)$ (1)	
	Depth considered as constant in the reservoir	H	Variable used for expressing the dimensions of the problem	
	Roughness	ε	$\Pi_5 = \varepsilon / H$	
	Characteristic frequency of the jet	f	$\Pi_6 = fH^2 / Vb \times \Pi_3 \Pi_2^{-1} = fH / V = \mathsf{St}$	Strouhal (2)
	Characteristic longitudinal length of the jet	Λ_x	$\Pi_7 = \Lambda_x / H$	
	Characteristic lateral length of the jet	Λ_y	$\Pi_8 = \Lambda_y / H$	
	Gravity acceleration	g	$\Pi_9 = \sqrt{Q^2 / \left(gH^5\right) \times \Pi_3^{-2} \Pi_2^2} = \mathsf{F}$	Froude
Fluid	Volume mass	ρ	Variable used for expressing the dimensions of the problem	
	Dynamic viscosity	μ	$\Pi_{10} = \rho V b / \mu \times 4R / b = \mathsf{R}$ (3)	Reynolds
	Surface tension	σ	$\Pi_{11} = \rho V^2 b^2 / \left(\sigma H\right) \times \Pi_3^{-2} \Pi_2^2 = \rho V^2 H / \sigma = \mathsf{W}$	Weber

(1) This dependent variable is used to express in a known formulation some Π-parameters.
(2) The Strouhal number is a non-dimensional number used for describing oscillating flow mechanism.
(3) In Π_{10}, $R=bH/(2H+b)$ corresponds to the hydraulic radius in the inlet channel.

Tab. 2 Geometry and hydraulic conditions of the data-set for the present experiments

Geometry				Hydraulic conditions				
L (m)	ΔB (m)	b (m)	SF	H (cm)	Q (L/s)	F	S	R×10⁻²
1.6	0.45	0.08	7.10	[1.7 - 7.3]	[0.13 - 2]	[0.09 - 0.45]	[0.02 - 0.11]	[78 - 562]
1.4	0.45	0.08	6.19	[1.0 - 6.0]	[0.13 - 1.5]	[0.09 - 0.51]	[0.02 - 0.22]	[80 - 500]
1.2	0.45	0.08	5.30	[1.2 - 7.7]	[0.13 - 2.5]	[0.08 - 0.47]	[0.02 - 0.19]	[72 - 657]
1	0.45	0.08	4.42	[1.2 - 5.8]	[0.13 - 1.5]	[0.10 - 0.47]	[0.02 - 0.18]	[83 - 546]
1	0.46	0.06	4.89	[1.4 - 6.8]	[0.13 - 1.5]	[0.13 - 0.46]	[0.02 - 0.15]	[84 - 445]
0.7	0.45	0.08	3.1	[0.9 - 5.3]	[0.13 - 1.5]	[0.11 - 0.53]	[0.02 - 0.24]	[86 - 593]

Tab. 3 Detailed geometric and hydraulic conditions of the thirty nine meandering flows

Geometry				Hydraulic conditions				
L (m)	Δ*B* (m)	*b* (m)	SF	*H* (cm)	*Q* (L/s)	F	S	R×10^{-2}
1.4	0.45	0.08	6.19	2.69	0.51	0.46	0.06	151
1.4	0.45	0.08	6.19	1.74	0.26	0.46	0.11	92
1.4	0.45	0.08	6.19	3.07	0.50	0.37	0.05	141
1.2	0.45	0.08	5.30	5.46	1.47	0.46	0.02	310
1.2	0.45	0.08	5.30	6.75	2.04	0.46	0.02	379
1.2	0.45	0.08	5.30	2.87	0.53	0.44	0.06	154
1.2	0.45	0.08	5.30	1.83	0.27	0.43	0.10	92
1.2	0.45	0.08	5.30	1.15	0.13	0.41	0.19	48
1.2	0.45	0.08	5.30	4.43	0.99	0.42	0.03	235
1.2	0.45	0.08	5.30	3.35	0.50	0.32	0.05	134
1.2	0.45	0.08	5.30	2.74	0.25	0.22	0.07	74
1.2	0.45	0.08	5.30	4.02	0.50	0.25	0.04	123
1.2	0.45	0.08	5.30	5.08	1.02	0.36	0.03	224
1.0	0.45	0.08	4.42	1.80	0.25	0.41	0.10	84
1.0	0.45	0.08	4.42	2.74	0.50	0.44	0.06	148
1.0	0.45	0.08	4.42	5.56	1.53	0.47	0.02	320
1.0	0.45	0.08	4.42	1.25	0.13	0.36	0.18	47
1.0	0.45	0.08	4.42	1.95	0.12	0.18	0.12	41
1.0	0.45	0.08	4.42	2.24	0.26	0.31	0.08	82
1.0	0.45	0.08	4.42	2.90	0.50	0.40	0.06	144
1.0	0.45	0.08	4.42	4.23	1.00	0.46	0.03	242
1.0	0.45	0.08	4.42	5.40	1.46	0.46	0.02	310
1.0	0.45	0.08	4.42	5.84	1.43	0.40	0.02	290
1.0	0.45	0.08	4.42	4.96	1.03	0.37	0.03	230
1.0	0.45	0.08	4.42	3.78	0.48	0.26	0.04	123
1.0	0.45	0.08	4.42	3.27	0.24	0.16	0.06	66
1.0	0.46	0.06	4.89	3.39	0.50	0.42	0.05	154
1.0	0.46	0.06	4.89	2.10	0.25	0.44	0.09	97
1.0	0.46	0.06	4.89	1.41	0.13	0.41	0.15	58
1.0	0.46	0.06	4.89	5.19	1.01	0.45	0.03	246
1.0	0.46	0.06	4.89	2.12	0.13	0.22	0.11	50
1.0	0.46	0.06	4.89	2.55	0.27	0.35	0.07	95
1.0	0.46	0.06	4.89	3.44	0.50	0.41	0.05	153
1.0	0.46	0.06	4.89	5.06	0.98	0.46	0.03	243
1.0	0.46	0.06	4.89	6.69	1.50	0.46	0.02	308
1.0	0.46	0.06	4.89	6.84	1.48	0.44	0.02	301
1.0	0.46	0.06	4.89	5.59	1.00	0.40	0.03	232
1.0	0.46	0.06	4.89	4.04	0.51	0.33	0.04	144
1.0	0.46	0.06	4.89	3.24	0.25	0.22	0.06	78

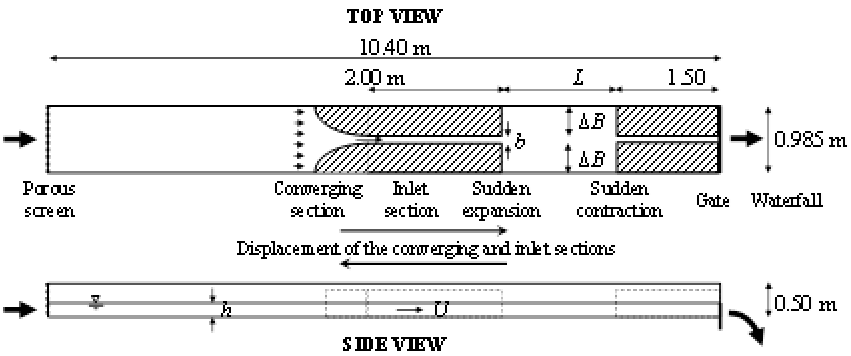

Fig. 1 Sketch of the experimental setup (adapted from Dufresne et al. [5]).

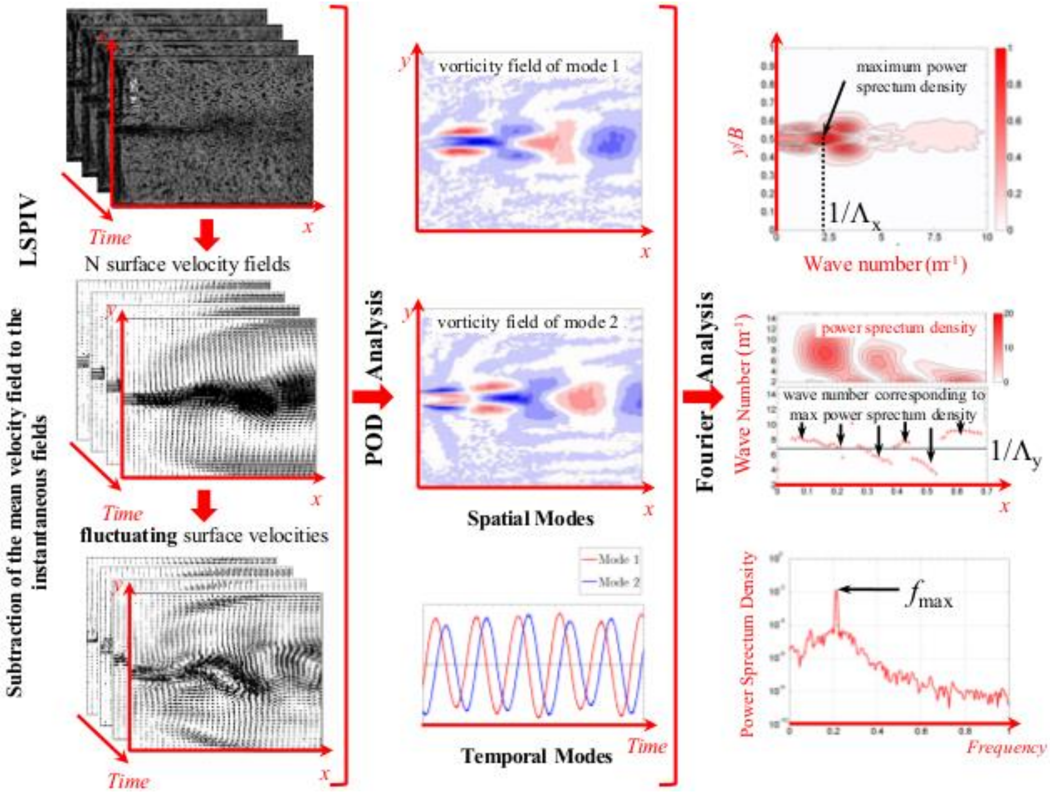

Fig. 2 Principles for extracting the characteristic lengths and frequency of the meandering jet

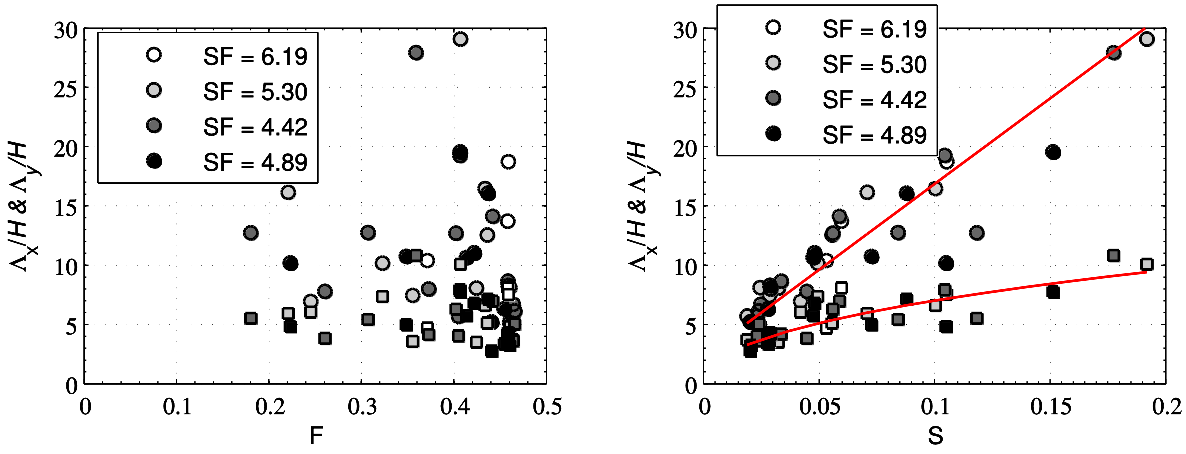

(a) (b)

Fig. 3 (a) Characteristics lengths Λ_x/H (□) and Λ_y/H (○) plotted with respect to F, for various SF. (b) Λ_x/H (□) and Λ_y/H (○) as a function of S. S follows Eq. 6 and Eq. 7.

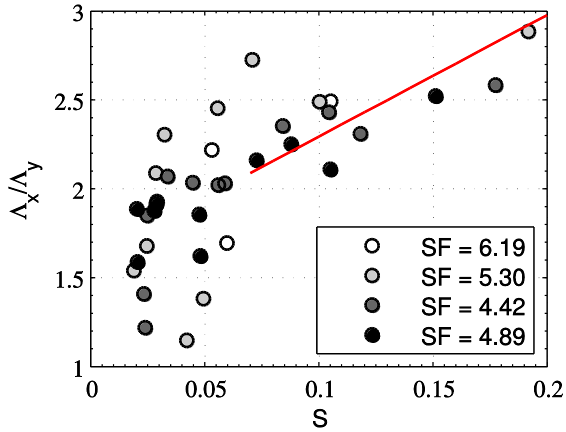

Fig. 4 Ratio of Λ_x and Λ_y plotted with respect to S, for various SF. Λ_x/Λ_y follows Eq. 8.

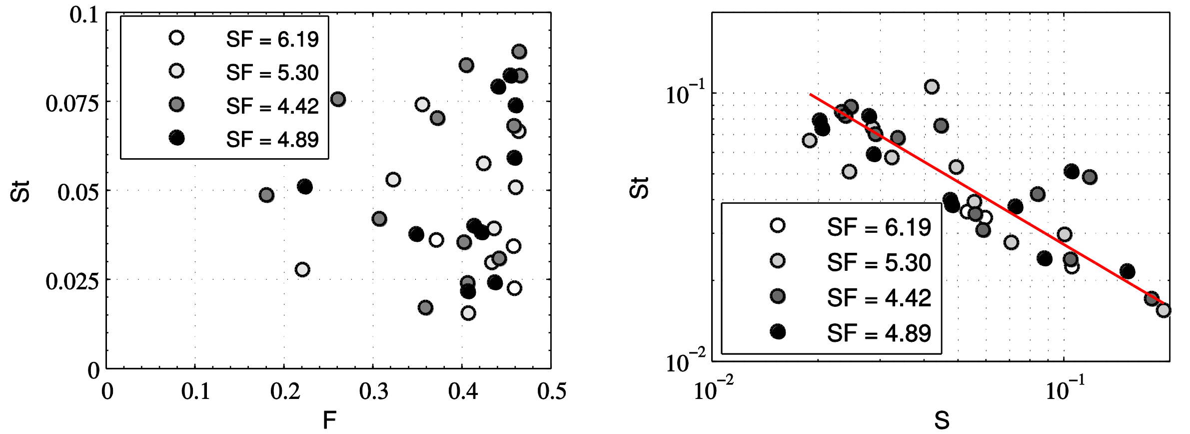

(a) (b)

Fig. 5 (a) Strouhal number, St, plotted with respect to the Froude number F for various shape factor, SF. (b) St plotted relative to the friction number S. St follows Eq. 9.

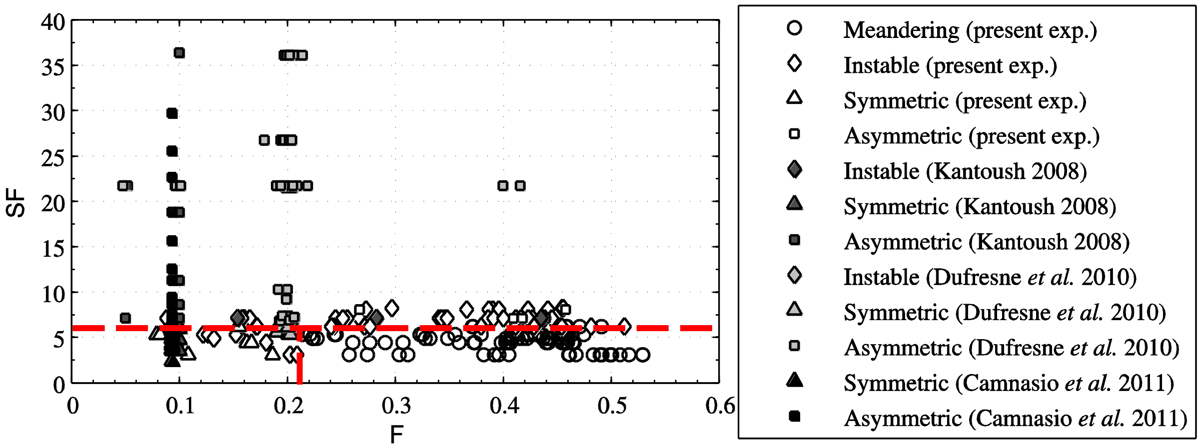

Fig. 6 Representation of the different flow regimes in shallow rectangular reservoirs as a function of SF and F. The horizontal dashed line reference SF = 6.2 and the vertical dashed line F = 0.21.